*Nano Research* 2015, 8(3): 907–919
DOI 10.1007/s12274-014-0572-2
**Research Article**
ISSN 1998-0124
CN 11-5974/O4

# Self-assembled vertically aligned gold nanorod superlattices for ultra-high sensitive detection of molecules

Amey Apte[1], Prashant Bhaskar[1], Raja Das[2,3], Smita Chaturvedi[1], Pankaj Poddar[2,3], and Sulabha Kulkarni[1] (✉)

[1] *Indian Institute of Science Education and Research (IISER), Homi Bhabha Road, Pashan, Pune – 411008, India*
[2] *Physical and Materials Chemistry Division, CSIR-National Chemical Laboratory, Pashan, Pune – 411008, India*
[3] *Academy of Scientific and Innovative Research (AcSIR), Anusandhan Bhavan, 2 Rafi Marg, New Delhi – 100001, India*

**Received:** 5 May 2013
**Revised:** 25 August 2014
**Accepted:** 26 August 2014



**KEYWORDS**
nanostructures,
self-assemblies,
superlattices,
Raman spectroscopy,
sensors

## ABSTRACT

We show that self-assembled vertically aligned gold nanorod (VA-GNRs) superlattices can serve as probes or substrates for ultra-high sensitive detection of various molecules. D-glucose and 2,4,6-trinitrotoluene (TNT) have been chosen as model systems due to their very low Raman cross-sections ($5.6 \times 10^{-30}$ cm$^2$·molecule$^{-1}$·sr$^{-1}$ for D-glucose and $4.9 \times 10^{-31}$ cm$^2$·molecule$^{-1}$·sr$^{-1}$ for TNT) to show that the VA-GNR superlattice assembly offers as low as yoctomole sensitivity. Our experiment on mixed samples of bovine serum albumin (BSA) and D-glucose solutions demonstrate sensitivity for the latter, and the possible extension to real samples. Self-assembled superlattices of VA-GNRs were achieved on a silicon wafer by depositing a drop of solvent containing the GNRs and subsequent solvent evaporation in ambient conditions. An additional advantage of the VA-GNR monolayers is their extremely high reproducible morphology accompanied by ultrahigh sensitivity which will be useful in many fields where a very small amount of analyte is available. Moreover the assembly can be reused a number of times after removing the already present molecules. The method of obtaining VA-GNRs is simple, inexpensive and reproducible. With the help of simulations of monolayers and multilayers it has been shown that superlattices can achieve better sensitivity than monolayer assembly of VA-GNRs.

## 1 Introduction

Ultrasensitive detection of molecules is necessary in various fields like medicine, forensics, pollution analysis, and security applications [1–4]. Raman scattering spectroscopy has become a very well-established molecular fingerprinting technique due to its high selectivity and accurate measurement capability of molecular vibration frequencies and their changes in different chemical surroundings. However,

Address correspondence to s.kulkarni@iiserpune.ac.in

Raman scattering cross-sections are inherently very small [5–8]. Therefore, laser beams of appropriate wavelength and high power need to be used. It was found about four decades ago that it is possible to enhance the Raman signal using rough silver or gold substrates [9, 10]. Since then the search for more and more sensitive (reaching single molecule detection level), easy to prepare and cost-effective substrates for Raman spectroscopy continued. The use of gold or silver nanostructures with different shapes, speckled silica–gold core–shell particles, as well as shell-isolated nanoparticles gave large enhancement factors for the Raman signals [11–14]. The Raman signal enhancement, known as surface enhanced Raman spectroscopy (SERS), can be chemical or electromagnetic, or a combination of both effects. In the chemical effect, a charge transfer complex is formed between the molecules and the substrate, whereas electromagnetic enhancement originates due to localized surface plasmon resonance (SPR). While the chemical enhancement is molecule specific, electromagnetic enhancement by creation of "hot spots" is substrate dependent and can occur for any molecule and therefore its use predominates.

Recently, femtomolar sensitivity was obtained for 1,2-bis(4-pyridyl)ethylene using a complex substrate of gold coated carbon nanotubes with high dielectric constant material (hafnia) as a SERS probe [8]. However, a major drawback of such substrates is their complex synthesis procedure and poor reproducibility. This can be overcome by using lithographically prepared Raman substrates [15–17]. Duyne's group has successfully used nano sphere lithography (NSL) for preparing SERS substrates [5]. Although, such substrates have been quite successful, leading to single molecule sensitivity, the major challenge in their fabrication is the large number of steps needed for fabrication and the increased material cost, along with complicated processes.

Another alternative is to use self-assembly of nanomaterials to enhance the Raman signals. For SERS, self-assembled GNRs are preferred due to facile tuning of the longitudinal SPR [18, 19]. GNRs can be prepared by a simple and well established seed mediated, surfactant protected method, and can be produced as monodisperse and aspect ratio-controlled particles by wet chemical procedures [20, 21]. Various types of self-assemblies, such as end-to-end, ring, and side-by-side, have been reported for GNRs [22–26]. Methods to create regular and reversible self-assemblies used for nanoparticles are applicable to GNRs as well [27]. Even in multilayers, it is observed that every self-assembly has a different morphology and is unlikely to give the same pattern, and hence, the same result. This problem can be overcome by obtaining self-assembled vertically aligned gold nanorods (VA-GNRs) superlattices in which one always obtains a unique hexagonal arrangement of GNRs, and hence reproducible structures. Here we demonstrate that the VA-GNR superlattices can increase the sensitivity up to the yoctomole level for molecules with extremely low Raman cross-sections.

## 2 Results and discussion

In this work we have obtained VA-GNR superlattices using evaporation of a liquid drop containing GNRs. This produces hexagonally close-packed large (a few tens of $\mu m^2$) arrays, irrespective of their aspect ratio [28–30].

### 2.1 Self-assembled superlattices of vertically aligned gold nanorods

Figure 1(a) illustrates the UV–vis absorption spectrum of GNRs in solution and Fig. 1(b) the field emission scanning electron microscope (FESEM) image of GNRs drop-cast on a silicon substrate using the same solution. The rods are lying in the plane of the silicon substrate. All the FESEM images were acquired at 3 kV operating voltage. GNRs were synthesized using the seed-mediated growth method [20, 21]. It can be seen that monodisperse GNRs of diameter ~8.9 nm and length ~34.2 nm are obtained, thus equating to an aspect ratio of ~3.8. The SPR peaks for the same sample obtained at wavelengths of 540 nm and 722 nm are attributed to the transverse and longitudinal modes respectively. Zeta potential measurements showed that the GNRs were positively charged (+70 mV).

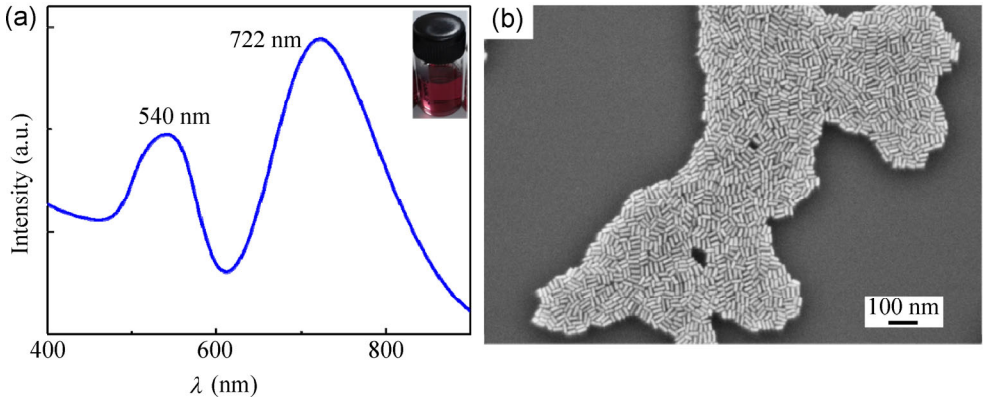


**Figure 1** (a) UV–vis absorption spectrum of the GNR solution with a photograph of the solution in the inset. (b) FESEM image of GNRs.

A drop of the solution (see the Experimental Section) was placed on a polished silicon substrate and allowed to dry at ambient temperature and pressure for three days. The FESEM images obtained in several parts of the substrate showed large arrays of VA-GNRs similar to those reported earlier [28–30]. The entire procedure followed for obtaining the VA-GNRs is illustrated in Fig. 2 (also see the Experimental Section).

Figure 3(a) depicts an FESEM image obtained on an area of ~17.8 μm$^2$, in one of the regions on the substrate. Consistent with some earlier reports, self-assembled VA-GNRs were mostly obtained at the edges of the liquid drop (coffee rings). From the precursor solution several substrates were made, which always showed vertical self-assembly of GNRs. The FESEM image in Fig. 3(b) was taken after tilting the sample stage and showed that superlattices of VA-GNRs have been formed. Superlattices of VA-GNRs also have been reported earlier [31, 32]. Figure 3(c) depicts a small section of the same material. The separation between adjacent GNRs was found to be ~3 nm, sufficient for the creation of hot spots or electric field enhancement [29]. A Fourier transform of the FESEM images depicts a hexagonal pattern, as shown in Fig. 3(d). It indicates that there is a long-range order in the self-assembly of the VA-GNRs. More detailed FESEM investigations of the samples showed the presence of Moiré patterns, which is discussed in Section 2.3.

The advantage of these assemblies is the facile method of synthesizing GNRs using cetyltrimethyl-ammonium bromide (CTAB) as the surfactant. Even gemini surfactants have been successfully used by

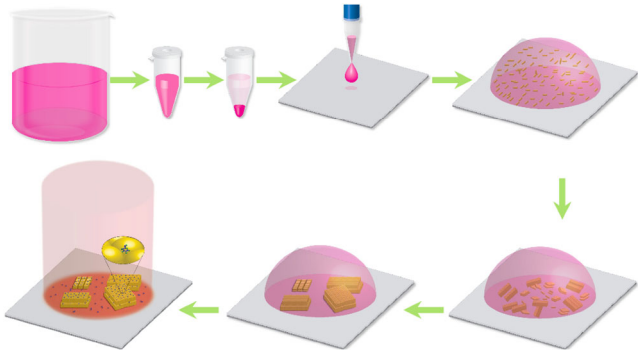

**Figure 2** Formation of vertically aligned gold nanorod arrays via evaporation-induced slow assembly.

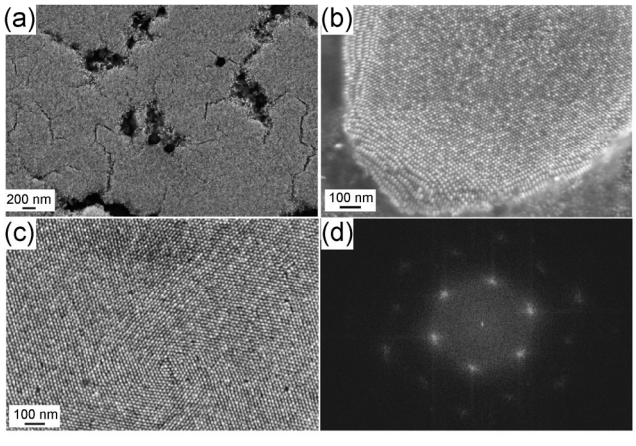


**Figure 3** (a) FESEM image of a large area of VA-GNR array. (b) Close-up view showing multilayers. (c) FESEM image showing close-packed arrangement. (d) 2D FFT of the vertical array showing hexagonal close-packed, long-range order.

Liz-Márzan's group to obtain VA-GNRs or multi-layered hexagonal superlattices [31]. As illustrated here, achieving such superlattices is very simple and straightforward. A drop of the concentrated liquid

containing GNRs is placed on any desired substrate like glass, silicon, ITO-coated glass, or any other flat surface and allowed to slowly evaporate at ambient conditions. A number of large islands (a few tens of $\mu m^2$) of VA-GNR superlattices can be observed in the FESEM images, within the so-called "coffee ring" of the drop. The VA-GNR superlattices form long-range hexagonal arrays. These assemblies are mostly observed at the periphery of the drop. It is possible to use lithographically patterned substrates to deposit VA-GNRs by a similar drop-cast method [32]. The self-assembly due to solvent evaporation occurs at ambient pressure and temperature, attributed to a balance between the attractive van der Waals interaction, capillary action and the repulsive forces between the CTAB molecules, hexa-alkanethiol or molecules like gemini surfactants [28–30]. Peng et al. and Xie et al. have proposed that some extent of self-assembly of GNRs in the form of a hexagonal arrangement could take place in the liquid drop itself, before it settles on the substrate to form larger arrays [28]. Although Xie et al. stated that GNRs with CTAB surfactant capping cannot form ordered vertical arrays through evaporation-induced self-assembly due to the large electrostatic repulsive forces (~50–60 mV) [30], Peng et al. have reported formation of monolayers of self-assembled VA-GNRs with CTAB capping via the same evaporation-induced method [28]. The latter group explained that the large electrostatic repulsive force between two GNRs due to the CTAB layers can be stabilized by the depletion and van der Waals' forces, both of which are attractive in nature. The synergy between these forces is purported to ultimately result in the formation of such extensive arrays. Moreover, Peng et al. have obtained such VA-GNR arrays in monolayer fashion, in the form of "coffee-rings" on arbitrary substrates [28]. Following a similar procedure of evaporation-induced self-assembly, we have obtained repeated instances of VA-GNR multilayers. A probable reason for the occurrence of such multilayers could be as follows: GNRs assemble in the form of nuclei before complete evaporation of the solvent drop. According to Peng et al., the nuclei grow into monolayers which stand up on the substrate due to surface energy minimization [28]. Further, a monolayer from the solution phase has a probability of stacking vertically on top of another monolayer already on the substrate. This process can continue and ultimately result in the formation of multilayers of VA-GNR arrays. Such a vertical stacking can occur due to a synergistic balance between the attractive depletion and van der Waals' forces and the repulsive electrostatic force due to CTAB molecules. Moreover, the density of CTAB molecules at the ends of GNRs is much less than that on their sides; this further results in a lowering of the electrostatic repulsion between the end–end stacking of VA-GNRs, and thus preferentially leads to the formation of multilayer arrays. Although, further investigations would be necessary to understand the mechanism of seed or nuclei formation in solvent evaporation induced assembly, the reproducibility of hexagonal VA-GNRs, as well as their superlattices, has led them to become very attractive SERS probes. Interestingly, surfactants like CTAB can be removed by UV–ozone treatment without damaging the orientation or positions of the GNRs as reported in Ref. [29], but Peng et al. showed that the distance between the GNRs in a monolayer can be varied by changing the ionic strength of the liquid drop [28]. Without altering the ionic strength, one typically gets a distance between the two GNRs of ~3 nm, corresponding to the thickness of the CTAB layer. The Liz-Márzan group demonstrated the detection of prions, a large molecule in biological media, using VA-GNR superlattices and Peng et al. detected food contaminants like phthalates and melamine with femtomolar sensitivity using monolayers of VA-GNRs [28, 29].

Here, we have used the self-assembled VA-GNR superlattices to show that D-glucose and 2,4,6-trinitrotoluene (TNT) can be detected with sensitivity much higher than a single layer of VA-GNRs. Although such self-assemblies have proven to be excellent in the detection of prions, further experiments on the detection of other organic molecules are quite important because the sensitivity for different molecules may differ since Raman cross-sections vary for different molecules [28, 29]. For normal Raman scattering (NRS), the cross-sections for D-glucose and TNT are $5.6 \times 10^{-30}$ $cm^2 \cdot molecule^{-1} \cdot sr^{-1}$ and $4.9 \times 10^{-31}$ $cm^2 \cdot molecule^{-1} \cdot sr^{-1}$ respectively [33–35]. These values are comparable to the cross-sections of molecules

used by Peng et al. [28]. However, we show here that the use of VA-GNR superlattices shows greater detection sensitivity compared to a monolayer of VA-GNRs.

According to the 2013 report of World Health Organization, there are 347 million people worldwide who are victims of diabetes mellitus. This number is expected to almost double by 2,035! It is known that uncontrolled diabetes increases the glucose level in blood circulation, affecting the nervous system and is a major cause of failure of organs such as eyes, kidneys, and heart. Although, it is not possible at present to cure diabetes, the regular monitoring of glucose levels in the body and administration of appropriate doses of insulin or medication can keep diabetes under control, thus increasing the longevity of the patients as well as keeping normal health. Therefore, glucose-level monitoring amongst diabetic patients, as well as early checks for diabetes among healthy persons, is very important. The common glucose-level monitoring methods involve taking a blood sample and analyzing it chemically, enzymatically (electrochemical or amperometric means), colorimetrically or spectroscopically [36, 37]. Detection of glucose by electrochemical methods, in which glucose is oxidized on a glucose oxidase ($GO_x$) covered substrate to obtain hydrogen peroxide, which in turn produces an electric current using various nanomaterials has been discussed by Claussen et al. [38]. It was reported that glucose sensitivity up to 0.3 μM concentration can be achieved. Yang et al. developed a photonic crystal fiber to sense small concentrations of glucose using Raman spectroscopy [39]. In recent years, attempts have been made to improve and devise new SERS substrates to achieve high accuracy and sensitivity for glucose detection. However, the SERS cross-sections are inherently very low and long data acquisition times, along with the high laser power, becomes mandatory. Therefore, it is important to enhance the Raman signal for accurate and quick or even continuous monitoring of body glucose levels.

We demonstrate here that SERS can be used to detect pure D-glucose with yoctomole-level accuracy. This will allow glucose detection even in saliva or tears where glucose levels are much less than those in blood. This could be done with ultra-high sensitivity requiring minimal amount of body fluids. It should be noted that we use pure D-glucose in our experiments. Samples containing glucose from human body fluids or other animals would contain other bio-molecules which could give signals which overlap with the glucose signal, making unambiguous estimation doubtful. However we believe that it is necessary at this stage to show how the molecule detection capability of SERS substrates can be enhanced. The applications of such a methodology would certainly need further experiments, and is a challenging task which needs to be taken further if one is convinced that the method is indeed extremely sensitive and gives sufficiently strong signals against a background of other signals.

### 2.2 Surface-enhanced Raman spectroscopy experiments

Self-assembled VA-GNR superlattices discussed above, were used for SERS experiments. The spectra were obtained using a He–Ne laser ($\lambda$ = 632.8 nm, 2 μm spot diameter, at 20 mW power). Each spectrum was recorded in 2 s, after complete solvent evaporation. Figure 4(a) shows the SERS spectra after treating the VA-GNR arrays with UV–ozone and after complete drying of 4 μL of pure ethanol solution. The UV–ozone treatment altered neither the self-assembly of VA-GNRs nor the inter-GNR separation, as confirmed by FESEM images (not shown here). The spectra do not show any peaks corresponding to CTAB after the UV–ozone treatment, nor peaks due to ethanol, over the entire region of the Raman spectra (1,000–1,500 $cm^{-1}$) recorded here. In Fig. 4(b), SERS spectra at various molar concentrations of D-glucose are shown. The spectra are normalized with respect to the peak at ~1,172 $cm^{-1}$. For D-glucose, peaks observed at 1,115 $cm^{-1}$ and 1,172 $cm^{-1}$ are attributed to (C–OH) and (C–C) stretching modes and (C–O–H) bending modes, whereas those at 1,291 $cm^{-1}$, 1,364 $cm^{-1}$ and 1,388 $cm^{-1}$ arise due to (O–C–H), (C–O–H), and (C–C–H) bending modes, and the peak at 1,431 $cm^{-1}$ can be attributed to the pure $CH_2$-vibration mode [40, 41]. However, Söderholm et al. [40] have observed the Raman peaks of glucose at 1,098 $cm^{-1}$, 1,125 $cm^{-1}$, 1,264 $cm^{-1}$, 1,340 $cm^{-1}$, and 1,373 $cm^{-1}$. The differences

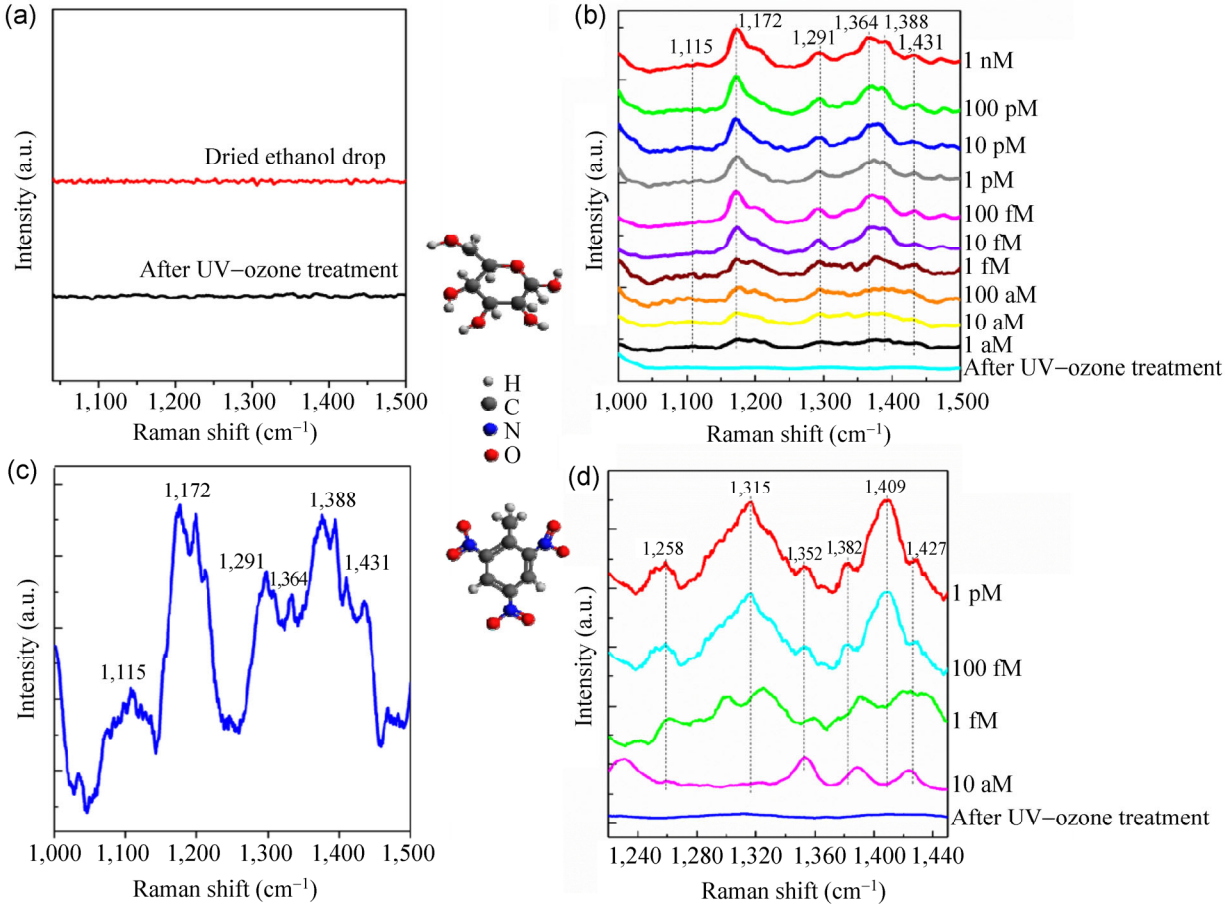


**Figure 4** (a) SERS spectra after UV–ozone treatment, and of the dried ethanol drop. (b) Spectra of 4 μL glucose solution dropcasts of concentrations 1 aM to 1 nM. (c) Spectrum of 1 aM glucose solution, and (d) spectra of 8 μL TNT solution dropcasts of concentrations 10 aM to 1 pM, on the VA-GNR arrays.

in the peak positions may arise due to different proximities between the adsorbate molecules and the substrate.

As the concentration was reduced from 1 nM to 1 aM, the intensity of all the peaks decreased, but the signatures of the glucose molecules were clearly visible even for 1 aM concentration (see Fig. 4(c)) Molarity calculations show that 4 μL of 1 aM D-glucose solution equates to 4 yoctomoles, which is equivalent to ~three D-glucose molecules. Thus, extremely high molecular sensitivity was achieved. SERS spectra checked after the cleaning showed that there were no signatures of glucose. Thus it is indeed possible to reuse the substrates.

In order to show that the assembly of VA-GNR superlattices is a generic SERS probe, we also tested them with a molecule of still lower Raman scattering cross-section, namely TNT. The procedure used for Raman scattering data acquisition for TNT solutions was exactly the same as for D-glucose solutions described above. The Raman spectrum of TNT is rich in vibrational modes due to presence of the aromatic ring, and the nitro and methyl groups, as reported earlier [42, 43]. Figure 4(d) depicts the SERS spectra recorded for TNT solutions. The modes observed at 1,258 $cm^{-1}$, 1,409 $cm^{-1}$ and 1,427 $cm^{-1}$ are attributed to ring stretching and $CH_3$ deformation. The peaks at 1,315 $cm^{-1}$, 1,352 $cm^{-1}$ and 1,382 $cm^{-1}$ are characteristic modes of TNT which could be attributed to 4-$NO_2$, 2,6-$NO_2$ and 2,4,6-$NO_2$ symmetric, and C–N stretching bands, respectively [42]. Sun et al. have reported the SERS spectra of TNT gas on Ag–$SiO_2$–CNT substrates [43]. They identified modes at 1,270 $cm^{-1}$, 1,358 $cm^{-1}$, and 1,434 $cm^{-1}$ besides the modes at 817 $cm^{-1}$ and 1,538 $cm^{-1}$. We recorded the SERS spectra in the range 1,220–1,450 $cm^{-1}$, in which all three vibrational modes

are observed as Raman shifts [44]. Our calculations show that 8 μL of 10 aM TNT solution corresponds to 80 yoctomoles, equivalent to ~48 molecules. The ultra-high sensitivity obtained for D-glucose and TNT molecules using VA-GNR superlattices for SERS can be understood as follows; Plasmonic hotspots are created in the gaps between gold/silver nanoparticles which enhance the local electric field. Attempts are often made to create a large number of such hotspots in order to increase the optical signal. However in some cases, the use of randomly distributed nanoparticles can increase the separation and hence attenuate the electric field in such hotspots. This adversely affects the optical signal. On the other hand, VA-GNRs offer extensive and uniformly distributed hotspots in gaps as small as ~3 nm, thus greatly enhancing the local electric fields. In addition, the gaps between two VA-GNRs exert a capillary force on analyte molecules in solution that increase their local concentration at such hotspots. We believe that the SERS spectra result from a pure electromagnetic enhancement, as there is no chemical bonding between the analyte molecules and the VA-GNR surfaces. Further, using simulations we show that the superlattices enhance the sensitivity due to increase in the field intensity. Peng et al. have used the approach of changing the gap-distance between the VA-GNR monolayer assembly by changing the ionic strength of the solution [28]. However this is more complicated than simply using superlattices. This makes VA-GNR superlattices a universal and ultra-highly sensitive SERS substrate.

To analyze the applicability of the technique in real samples we tested a 8% Bovine Serum Albumin (BSA) solution which resembles blood serum. An 8% of BSA solution was prepared and two different concentrations of D-glucose, i.e. 1 mM and 100 mM were added; these fall in the range of normal glucose levels in human plasma samples [45]. The Raman spectra of "BSA", "BSA + 1 mM D-glucose", and "BSA + 100 mM D-glucose" on VA-GNR substrates are shown in Fig. 5. SERS spectra of BSA on VA-GNR substrate does not show any enhancement of its Raman modes, which could be due to the large size of the BSA molecule (Stokes radius ($r_s$), 3.48 nm) [46]. Due to the large size of BSA molecules, they cannot

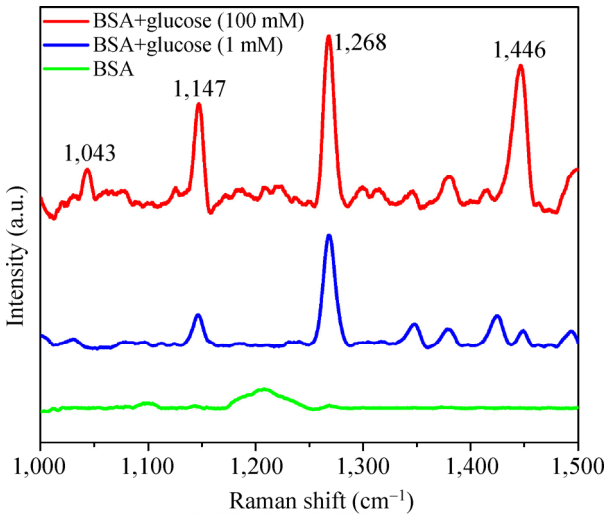


**Figure 5** SERS spectra of 8% BSA solution (green), BSA + glucose (1 mM) (blue) and BSA + glucose (100 mM) (red) (all 4 μL volume) on the VA-GNR arrays.

penetrate the gap between adjacent nanorods, where the electromagnetic hotspots are located in the VA-GNR arrays. On the other hand the significantly smaller size of the glucose molecules enables their penetration to the hot spots, resulting in their SERS signals.

Thus, in the case of "BSA + 1 mM D-glucose", and "BSA + 100 mM D-glucose" on VA-GNRs substrate, we could observe only enhancement of D-glucose signals, and not of BSA. Raman peaks at 1,043 $cm^{-1}$, 1,147 $cm^{-1}$, 1,268 $cm^{-1}$, and 1,446 $cm^{-1}$ were observed in our experiment on D-glucose solution. The shifts in the position of the Raman peaks could be due to change in the local dielectric environment of D-glucose molecules in the BSA solution. Our results clearly show that the VA-GNR substrates can be used for detecting glucose in serum samples, and even in blood samples.

### 2.3 Simulation by the finite element method

Peng et al. have previously used finite-difference time-domain (FDTD) simulations to study a monolayer of VA-GNR assembly [28], and Liz Márzan's group carried out FDTD simulations for three layers of VA-GNRs [29]. In order to further understand why there is an enhancement in the Raman signal, we have simulated the electric field associated with the vertically aligned gold nanorods arranged in a bilayer.

The layers were also rotated azimuthally with respect to each other. This is because we observed Moiré patterns which are discussed here. Figure 6 shows the results of finite element method simulations for GNR bilayer, which helps in understanding the basis of the SERS effect. Figure 6(a) depicts the top view of the GNRs with two layers of GNRs rotated about the $z$-axis through an angle of 30° and Fig. 6(b) shows the three-dimensional (3D) view of the assembly. A plane electromagnetic wave polarized in the $y$-direction with a vacuum wavelength of 524 nm was normally incident upon the GNRs. The GNRs were modeled with a dielectric permittivity $\varepsilon_1 = -3.94$ and $\varepsilon_2 = 2.58$ [47], while the substrate was assigned a constant refractive index of 1.5, characteristic of $SiO_2$. Figures 6(c) and 6(d) show uniform enhancement factors as large as ~$10^9$. Considering the central nanorod in the hexagonal cell located at the origin, four vertical lines parallel to the $z$-axis (and along the rod lengths) are drawn in the gap between the nanorods in the first $xy$-quadrant, located at azimuthal angles ($\phi$) 0°, 30°, 60°, and 90°. For simplicity, these lines are shown as black dots in Fig. 6(a).

To elucidate the plasmonic enhancement in the hotspots, normalized electric field intensities are extracted along these lines and plotted as a function of the $z$-height above the substrate in Fig. 6(e). For a better understanding, we can divide the abscissa into two regions, from $z$ = 0 to 40 nm, and from $z$ = 41 to 80 nm; these regions correspond to the two monolayers,

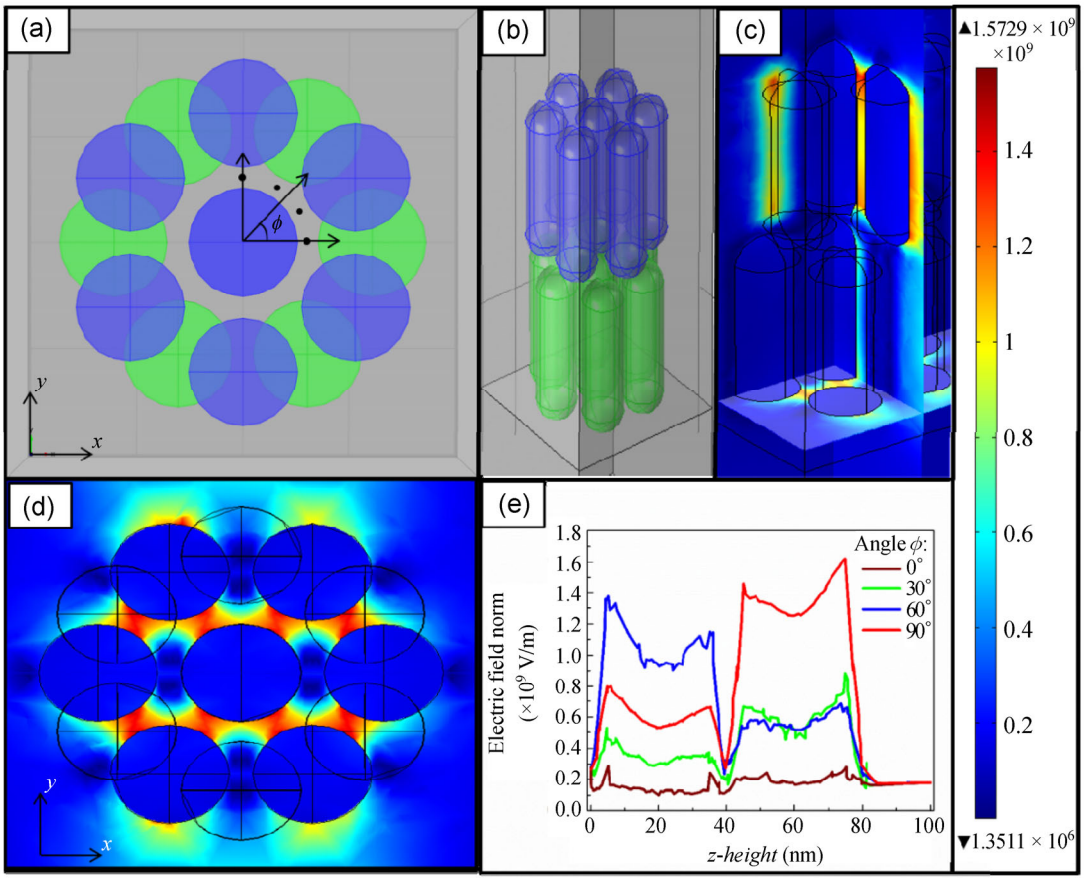


**Figure 6** (a) Top view of the hexagonally arranged GNR bilayer unit cell rotated by a relative azimuthal angle $\phi$ = 30°, on a silica substrate; the lower layer is shaded green and the upper one blue, for the sake of clarity. The distance between two adjacent rods is 2 nm. (b) 3D view of the construction; the bilayer is in the $xy$-plane with the rods pointing in the $z$-direction. (c) Normalized electric field color map with enhancement within the gaps in 3D view, and $xy$-plane and (d) at a height 5 nm above the substrate. (e) Values extracted along lines (depicted as black dots) parallel to the $z$-axis and located in the first $xy$-quadrant at azimuthal angles $\phi$ = 0°, 30°, 60°, and 90°.

since the height of each rod is taken to be 40 nm. For region 1, the highest enhancement can be seen for the vertical line at $\phi$ = 60° (blue curve). This is explained by the fact that the line lies between adjacent vertical nanorods in the lower monolayer. The line at $\phi$ = 90° (red curve) experiences more enhancement than the line at $\phi$ = 30° (yellow curve) since the former one is located in the *y*-axis and is therefore closer to the sense of direction of incident polarization. Hence, the electric field there is subject to greater enhancement.

For region 2, the enhancement is a maximum for the vertical line at $\phi$ = 90°, followed by the one at $\phi$ = 30°. Since the former line lies between adjacent vertical nanorods in the upper monolayer and is now fully in the sense of direction of the incident polarization, the electric field gets enhanced the most. This is followed by the line at $\phi$ = 30°, which although not fully in the sense of direction of the incident polarization, is nevertheless between two vertical nanorods of the upper monolayer. The line at $\phi$ = 0° (green curve) experiences the least enhancement of all simply because it is located on the *x*-axis and hence furthest away from the sense of direction of incident polarization, for all cases.

In Fig. 7 the zoomed out FESEM image shows several regions where Moiré patterns appear. Such Moiré patterns were also reported for VA-GNR superlattices by Liz-Márzan's group in the supplementary material, without any discussion [31]. A Moiré pattern is formed when two distinct periodicities are superimposed, with a slight misalignment. The result is the appearance of a third "spoof" periodicity, which is dubbed the Moiré pattern. In Fig. 7(a) the patterns can be seen in many regions as alternating "zebra" like stripes of bright and dark contrast on the gold nanorod islands. The basis of a Moiré pattern is illustrated in Fig. 7(b). Suppose the two superimposed periodic lattices have vectors $\boldsymbol{k}_1$ and $\boldsymbol{k}_2$. The Moiré periodicity is then given as

$$\boldsymbol{k}_{\text{Moiré}} = \boldsymbol{k}_1 - \boldsymbol{k}_2$$

In the case of this work, the reason behind the appearance of Moiré patterns can be explained as follows: the vertically aligned nanorod arrays show exceptionally close-packed long range periodic order. When present in multilayers, the periodicities of the layers stacked above one another with a mutual azimuthal rotation and interact to give the Moiré patterns in the FESEM image.

Although the simulations carried out by Peng et al. and Liz-Márzan's group involve nanorods of different sizes and spacings, we have clearly demonstrated here that multilayer assembly in GNR superlattices offers better enhancement and higher sensitivity even down to the yoctomole level. Thus, a uniform hexagonal close-packed self-assembly of VA-GNRs indeed supports field enhancement and hence can be used as an excellent substrate for SERS detection experiments.

## 3 Conclusions

Vertically aligned, self-assembled superlattices of five layers of gold nanorods were obtained over large areas

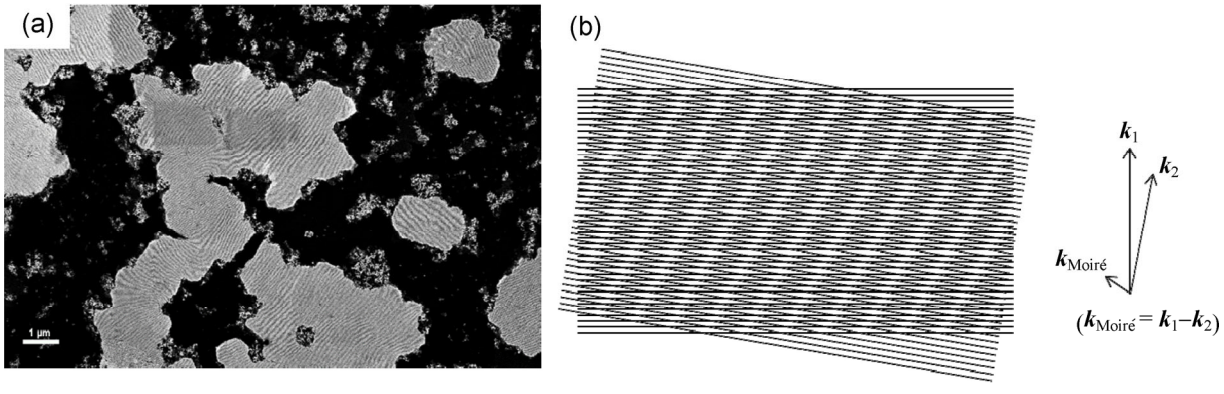


**Figure 7** (a) Zoomed out FESEM image of VA-GNRs exhibiting Moiré patterns in many regions. (b) Schematic illustration of the Moiré pattern.

on polished silicon substrates. Moiré patterns also were detected due to the rotation of the interlayers and their effect on the electrical field enhancement has been simulated for a bilayer assembly. The superlattices served as excellent SERS probes with ultra-high sensitivity down to yoctomole levels amounting to the detection of around three D-glucose molecules, the highest sensitivity reported so far using VA-GNRs for any molecules; this is attributed to the presence of VA-GNR superlattices. A still lower Raman scattering cross-section molecule viz. TNT was also detected up to few tens of yoctomoles at moderate laser power, implying that the VA-GNR superlattices have consistently ultra-high sensitivity and are generic substrates. Our experiment on mixed samples of BSA and D-glucose solutions—which mimic real serum samples—demonstrates SERS sensitivity for D-glucose, and thus paves the way towards possible extension to real samples. Finite element method simulations for the VA-GNR bilayer showed the electric field enhancement arising out of the mutual azimuthal rotation of the layers. The mutual azimuthal rotation of the bilayer also is important in understanding the presence of hotspots in the VA-GNR arrays, as well as the presence of Moiré patterns. Owing to their hexagonal arrangement, the VA-GNRs always generate the same pattern and hence reproducible results. The substrates were robust and simple to obtain. It would be interesting in future to investigate the effect of the concentration of the GNR solution and their aspect ratio on the self-assembly, as well as to optimize them for ultra-sensitive detection of various other analytes. Further work on the systematic control of the number of layers in the superlattices, their effect on the sensitivity of detection, along with the mechanism of formation VA-GNR assemblies (particularly whether the nucleation occurs on the substrate or in the liquid phase itself) needs to be carried out and will be addressed in the future. Besides their use as ultrasensitive detectors of molecules, VA-GNR assemblies have great potential in understanding coupled exciton–plasmon interactions as recently demonstrated in Ref. [48] and this should also be pursued.

# 4 Methods

## 4.1 Materials

Gold chloride hydrate ($HAuCl_4.xH_2O$), cetyltrimethylammonium bromide (CTAB), benzyldimethylhexadecylammonium chloride (BDAC), ascorbic acid, and D-glucose were purchased from Sigma Aldrich. Silver nitrate ($AgNO_3$) was purchased from Merck. Sodium borohydride ($NaBH_4$) was purchased from SRL Chem Pvt. Ltd, India. All chemicals were used without further purification. For all the experiments, Millipore™ Milli-Q water was used.

## 4.2 Preparation of CTAB-stabilized GNRs

The GNRs were synthesized via a two-step seed mediated growth method at room temperature [20]. In a typical reaction, the seed solution was prepared by mixing CTAB (0.2 M, 5 mL) and $HAuCl_4$ ($5 \times 10^{-4}$ M, 5 mL). After gentle stirring, freshly prepared ice-cold $NaBH_4$ (0.01 M, 0.6 mL) was added, followed by vigorous stirring for two minutes. This caused the colour of the solution to turn brownish-yellow.

The growth solution consisted of a binary surfactant solution of CTAB (0.2 M, 2.5 mL) and BDAC (0.15 M, 2.5 mL). To this, $AgNO_3$ (0.004 M, 0.2 mL) was added, followed by addition of a solution of $HAuCl_4$ (0.001 M, 5 mL) with gentle mixing. This caused the solution to turn golden yellow. Ascorbic acid (0.0788 M, 0.07 mL) was then added with shaking, which caused the resulting solution to turn colorless. Finally, 20 μL of the seed solution was added into the growth solution, and the latter was kept overnight at room temperature. A dark magenta color of the growth solution indicated successful formation of GNRs (Fig. 1(a)).

1 mL of the above solution was centrifuged thrice at 9,600 RPM for 20 min periods, with intermediate re-dispersion of the GNR precipitate in water to remove the excess surfactants and spherical nanoparticles. After the third round, the precipitate was dispersed in 50 μL of water to prepare a concentrated solution. 5 μL of this solution was drop-cast on a clean silicon wafer kept in a glass Petri dish sealed with Parafilm™ at 21 °C, to achieve the self-assembly induced by slow evaporation.

### 4.3 Preparation of glucose and TNT solutions

1.801 mg of D-glucose was dissolved in 10 mL of ethanol in a glass vial to make a 1 mM solution. In another vial, 2.271 mg of TNT was dissolved in 10 mL of ethanol, to make a 1 mM solution. Successive solutions with one-tenth the previous concentration were prepared by withdrawing 0.1 mL of the previous solution and dissolving it in 0.9 mL of ethanol. In this manner, D-glucose and TNT solutions of concentration from 1 nM down to 1 aM (in steps of 1/10) were prepared for the SERS detection experiments.

### 4.4 Preparation of BSA solutions

BSA solutions were prepared by dissolving 800 mg of BSA in 10 mL of water. D-glucose was then dissolved to prepare 1 mM and 100 mM solutions.

### 4.5 Characterization

UV–vis absorption spectra were recorded with a Perkin Elmer Lambda 950 UV–vis spectrophotometer. Scanning electron microscopy images were recorded with a Zeiss™ Ultra Plus field-emission scanning electron microscope at 3 kV operating voltage. Raman spectra were recorded with a Horiba Jobin Yvon LabRAM HR800 micro-Raman spectrophotometer fitted with a 632.8 nm He–Ne laser operating at 20 mW in back-scattering mode, with a 50X LD objective lens and 2 s acquisition times.

## Acknowledgements

We thank the Department of Science and Technology (DST), India Nano-Mission Initiative Project SR/NM/NS-42/2009. S.C. thanks DST, India Grant No SR/WOS/-A/PS50/2012(G). S.K. thanks UGC, India for constant support. The authors thank Anil Prathamshetti, IISER Pune, for technical assistance. P.P. acknowledges DST project DST/INT/ISR/P-8/2011.

## References

[1] Germain, M. E.; Knapp, M. J. Optical explosives detection: From color changes to fluorescence turn-on. *Chem. Soc. Rev.* **2009**, *38*, 2543–2555.

[2] Aragay, G.; Pons, J.; Merkoçi, A. Recent trends in macro-, micro-, and nanomaterial-based tools and strategies for heavy-metal detection. *Chem. Rev.* **2011**, *111*, 3433–3458.

[3] Salinas, Y.; Martínez-Máñez, R.; Marcos, M. D.; Sancenón, F.; Costero, A. M.; Parra, M.; Gil, S. Optical chemosensors and reagents to detect explosives. *Chem. Soc. Rev.* **2012**, *41*, 1261–1296.

[4] Thomas, S. W.; Joly, G. D.; Swager, T. M. Chemical sensors based on amplifying fluorescent conjugated polymers. *Chem. Rev.* **2007**, *107*, 1339–1386.

[5] Rodríguez-Lorenzo, L.; Alvarez-Puebla, R. A.; Pastoriza-Santos, I.; Mazzucco, S.; Stéphan, O.; Kociak, M.; Liz-Marzán, L. M.; García de Abajo, F. J. Zeptomol detection through controlled ultrasensitive surface-enhanced Raman scattering. *J. Am. Chem. Soc.* **2009**, *131*, 4616–4618.

[6] Camden, J. P.; Dieringer, J. A.; Zhao, J.; Van Duyne, R. P. Controlled plasmonic nanostructures for surface-enhanced spectroscopy and sensing. *Acc. Chem. Res.* **2008**, *41*, 1653–1661.

[7] Mathew, A.; Sajanlal, P. R.; Pradeep, T. Selective visual detection of TNT at the sub-zeptomole level. *Angew. Chem. Int. Ed.* **2012**, *51*, 9596–9600.

[8] Altun, A. O.; Youn, S. K.; Yazdani, N.; Bond, T.; Park, H. G. Metal-dielectric-CNT nanowires for femtomolar chemical detection by surface enhanced Raman spectroscopy. *Adv. Mater.* **2013**, *25*, 4431–4436.

[9] D. L. Jeanmarie, R. P. V. D. Surface Raman spectroelectrochemistry. Part I. Heterocyclic, aromatic, and aliphatic amines adsorbed on the anodized silver electrode. *J. Electroanal. Chem.* **1977**, *84*, 1–20.

[10] Albrecht, M. G.; Creighton, J. A. Anomalously intense Raman spectra of pyridine at a silver electrode. *J. Am. Chem. Soc.* **1977**, *99*, 5215–5217.

[11] Herrera, G.; Padilla, A.; Hernandez-Rivera, S. Surface enhanced Raman scattering (SERS) studies of gold and silver nanoparticles prepared by laser ablation. *Nanomaterials* **2013**, *3*, 158–172.

[12] Cao, Y. C.; Jin, R.; Mirkin, C. A. Nanoparticles with Raman spectroscopic fingerprints for DNA and RNA detection. *Science* **2002**, *297*, 1536–1540.

[13] Khurana, P.; Thatai, S.; Wang, P.; Lihitkar, P.; Zhang, L.; Fang, Y.; Kulkarni, S. K. Speckled $SiO_2$@Au core–shell particles as surface enhanced Raman scattering probes. *Plasmonics* **2012**, *8*, 185–191.

[14] Li, J. F.; Huang, Y. F.; Ding, Y.; Yang, Z. L.; Li, S. B.; Zhou, X. S.; Fan, F. R.; Zhang, W.; Zhou, Z. Y.; Wu, D. Y.; et al. Shell-isolated nanoparticle-enhanced Raman spectroscopy. *Nature* **2010**, *464*, 392–395.

[15] Mahajan, S.; Hutter, T.; Steiner, U.; Goldberg Oppenheimer, P. Tunable microstructured surface-enhanced Raman scattering substrates via electrohydrodynamic lithography. *J. Phys. Chem. Lett.* **2013**, *4*, 4153–4159.

[16] Wang, Y.; Lu, N.; Wang, W.; Liu, L.; Feng, L.; Zeng, Z.; Li, H.; Xu, W.; Wu, Z.; Hu, W.; et al. Highly effective and reproducible surface-enhanced Raman scattering substrates based on Ag pyramidal arrays. *Nano Res.* **2013**, *6*, 159–166.

[17] Gunnarsson, L.; Bjerneld, E. J.; Xu, H.; Petronis, S.; Kasemo, B.; Käll, M. Interparticle coupling effects in nanofabricated substrates for surface-enhanced Raman scattering. *Appl. Phys. Lett.* **2001**, *78*, 802–804.

[18] Huang, X.; Neretina, S.; El-Sayed, M. A. Gold nanorods: From synthesis and properties to biological and biomedical applications. *Adv. Mater.* **2009**, *21*, 4880–4910.

[19] Tiwari, N.; Yue Liu, M.; Kulkarni, S.; Fang, Y. Study of adsorption behavior of aminothiophenols on gold nanorods using surface-enhanced Raman spectroscopy. *J. Nanophotonics* **2011**, *5*, 053513.

[20] Nikoobakht, B.; El-Sayed, M. A. Preparation and growth mechanism of gold nanorods (NRs) using seed-mediated growth method. *Chem. Mater.* **2003**, *15*, 1957–1962.

[21] Li, N.; Zhao, P.; Astruc, D. Anisotropic gold nanoparticles: Synthesis, properties, applications, and toxicity. *Angew. Chem. Int. Ed.* **2014**, *53*, 1756–1789.

[22] Chen, H.; Shao, L.; Li, Q.; Wang, J. Gold nanorods and their plasmonic properties. *Chem. Soc. Rev.* **2013**, *42*, 2679–2724.

[23] Jana, N. R. Shape effect in nanoparticle self-assembly. *Angew. Chem. Int. Ed.* **2004**, *43*, 1536–1540.

[24] Jana, N. R.; Gearheart, L. A.; Obare, S. O.; Johnson, C. J.; Edler, K. J.; Mann, S.; Murphy, C. J. Liquid crystalline assemblies of ordered gold nanorods. *J. Mater. Chem.* **2002**, *12*, 2909–2912.

[25] Nikoobakht, B.; Wang, Z. L.; El-Sayed, M. A. Self-assembly of gold nanorods. *J. Phys. Chem. B* **2000**, *104*, 8635–8640.

[26] Sau, T. K.; Murphy, C. J. Self-assembly patterns formed upon solvent evaporation of aqueous cetyltrimethylammonium bromide-coated gold nanoparticles of various shapes. *Langmuir* **2005**, *21*, 2923–2929.

[27] Zhang, H.; Liu, Y.; Yao, D.; Yang, B. Hybridization of inorganic nanoparticles and polymers to create regular and reversible self-assembly architectures. *Chem. Soc. Rev.* **2012**, *41*, 6066–6088.

[28] Peng, B.; Li, G.; Li, D.; Dodson, S.; Zhang, Q.; Zhang, J.; Lee, Y. H.; Demir, H. V.; Ling, X. Y.; Xiong, Q. Vertically aligned gold nanorod monolayer on arbitrary substrates: Self-assembly and femtomolar detection of food contaminants. *ACS Nano* **2013**, *7*, 5993–6000.

[29] Alvarez-Puebla, R. A.; Agarwal, A.; Manna, P.; Khanal, B. P.; Aldeanueva-Potel, P.; Carbó-Argibay, E.; Pazos-Pérez, N.; Vigderman, L.; Zubarev, E. R.; Kotov, N. A.; et al. Gold nanorods 3D-supercrystals as surface enhanced Raman scattering spectroscopy substrates for the rapid detection of scrambled prions. *Proc. Natl. Acad. Sci. U.S.A.* **2011**, *108*, 8157–8161.

[30] Xie, Y.; Guo, S.; Ji, Y.; Guo, C.; Liu, X.; Chen, Z.; Wu, X.; Liu, Q. Self-assembly of gold nanorods into symmetric superlattices directed by OH-terminated hexa(ethylene glycol) alkanethiol. *Langmuir* **2011**, *27*, 11394–11400.

[31] Guerrero-Martínez, A.; Pérez-Juste, J.; Carbó-Argibay, E.; Tardajos, G.; Liz-Marzán, L. M. Gemini-surfactant-directed self-assembly of monodisperse gold nanorods into standing superlattices. *Angew. Chem. Int. Ed.* **2009**, *48*, 9484–9488.

[32] Xiao, J.; Li, Z.; Ye, X.; Ma, Y.; Qi, L. Self-assembly of gold nanorods into vertically aligned, rectangular microplates with a supercrystalline structure. *Nanoscale* **2014**, *6*, 996–1004.

[33] Shafer-Peltier, K. E.; Haynes, C. L.; Glucksberg, M. R.; Van Duyne, R. P. Toward a glucose biosensor based on surface-enhanced Raman scattering. *J. Am. Chem. Soc.* **2003**, *125*, 588–593.

[34] Ehlerding, A.; Johansson, I.; Wallin, S.; Östmark, H. Resonance-enhanced Raman spectroscopy on explosives vapor at standoff distances. *Int. J. Spectrosc.* **2012**, 158715.

[35] McCreery, R. L. *Raman Spectroscopy for Chemical Analysis*; John Wiley & Sons, Inc.: New York (USA), 2005.

[36] Wooten, M.; Shim, J. H.; Gorski, W. Amperometric determination of glucose at conventional vs. nanostructured gold electrodes in neutral solutions. *Electroanalysis* **2010**, *22*, 1275–1277.

[37] Rahman, M. M.; Ahammad, a. J. S.; Jin, J.-H.; Ahn, S. J.; Lee, J.-J. A comprehensive review of glucose biosensors based on nanostructured metal-oxides. *Sensors* **2010**, *10*, 4855–4886.

[38] Claussen, J. C.; Kumar, A.; Jaroch, D. B.; Khawaja, M. H.; Hibbard, A. B.; Porterfield, D. M.; Fisher, T. S. Nanostructuring platinum nanoparticles on multilayered graphene petal nanosheets for electrochemical biosensing. *Adv. Funct. Mater.* **2012**, *22*, 3399–3405.

[39] Yang, X.; Zhang, A.; Wheeler, D.; Bond, T.; Gu, C.; Li, Y. Direct molecule-specific glucose detection by Raman spectroscopy based on photonic crystal fiber. *Anal. Bioanal. Chem.* **2012**, *402*, 687–691.

[40] Söderholm, S.; Roos, Y. H.; Meinander, N.; Hotokka, M. Raman spectra of fructose and glucose in the amorphous and crystalline states. *J. Raman Spectrosc.* **1999**, *30*, 1009–1018.

[41] Yonzon, C. R.; Haynes, C. L.; Zhang, X.; Walsh, J. T.; Van Duyne, R. P. A glucose biosensor based on surface-enhanced Raman scattering: Improved partition layer, temporal stability, reversibility, and resistance to serum protein interference. *Anal. Chem.* **2003**, *76*, 78–85.

[42] Clarkson, J.; Smith, W. E.; Batchelder, D. N.; Smith, D. A.; Coats, A. M. A theoretical study of the structure and vibrations of 2,4,6-trinitrotoluene. *J. Mol. Struct.* **2003**, *648*, 203–214.

[43] Sun, Y.; Liu, K.; Miao, J.; Wang, Z.; Tian, B.; Zhang, L.; Li, Q.; Fan, S.; Jiang, K. Highly sensitive surface-enhanced Raman scattering substrate made from superaligned carbon nanotubes. *Nano Lett.* **2010**, *10*, 1747–1753.

[44] Sun, Z.; Ni, W.; Yang, Z.; Kou, X.; Li, L.; Wang, J. pH-Controlled reversible assembly and disassembly of gold nanorods. *Small* **2008**, *4*, 1287–1292.

[45] Agrawal, R. P.; Sharma, N.; Rathore, M. S.; Gupta, V. B.; Jain, S.; Agarwal, V.; Goyal, S. Noninvasive method for glucose level estimation by saliva. *J. Diabetes Metab.* **2013**, *4*, 266.

[46] Axelsson, I. Characterization of proteins and other macromolecules by agarose gel chromatography. *J. Chromatogr. A* **1978**, *152*, 21–32.

[47] Johnson, P. B.; Christy, R. W. Optical constants of the noble metals. *Phys. Rev. B* **1972**, *6*, 4370–4379.

[48] Peng, B.; Li, Z.; Mutlugun, E.; Hernandez Martinez, P. L.; Li, D.; Zhang, Q.; Gao, Y.; Demir, H. V.; Xiong, Q. Quantum dots on vertically aligned gold nanorod monolayer: plasmon enhanced fluorescence. *Nanoscale* **2014**, *6*, 5592–5598.